Plasma dynamics in a helicon thruster

Eduardo Ahedo
Universidad Politécnica de Madrid
ETS Ingenieros Aeronáuticos, Plaza Cardenal Cisneros, Madrid 28040, Spain

Abstract

Theoretical analyses of the internal and external dynamics of the plasma discharge in an helicon thruster are summarized. The internal dynamics studies cover the processes inside the thruster chamber: plasma production and heating, magnetic confinement, and subsonic flows. The external processes in the divergent magnetic nozzle are: the two dimensional plasma expansion and detachment, and the thrust gain. The formation of current-free double layers and its propulsive role are discussed too.

1. Introduction

Space plasma thrusters based on helicon sources are a subject of intensive current research[1, 2, 3, 4]. One of the principal projects, and genuinely European, is HPHCOM (Helicon Plasma Hydrazine Combined Micro), funded by the European Union within the 7th Framework Programme and conducted by a consortium of 15 institutions from 7 European countries. The main objective of the project is to design, test, optimize, and develop an helicon-based plasma thruster in the range 50-100 watts. The first phase of the project has been devoted to a deep theoretical investigation of the physics and critical parameters of helicon thrusters and the development of detailed numerical codes, that could guide in the thruster design and the interpretation of thruster tests in vacuum chambers. This paper is devoted to summarize the theoretical research carried out on the internal and external plasma dynamics in the helicon thruster.

2. Principles of operation

The main elements of a helicon thruster are (i) a feeding system that injects gas into a cylindrical vessel, (ii) a radiofrequency(RF) antenna system that emits helicon waves in the range 1-30 Mhz, (iii) a first set of magnetic coils surrounding the vessel, that creates a quasi-axial magnetic field required for an efficient plasma-wave energy absorption, and (iv) a second set of magnetic coils around the vessel exit, that configures a divergent magnetic nozzle. The helicon wave is part of the family of whistler waves[5].

There are two stages in an helicon thruster: the production stage inside the plasma source and the acceleration stage in the magnetic nozzle. Two types of processes take place inside the source: the resonant wave-plasma interaction, leading to the deposition of wave energy into the plasma and the multiple phenomena governing plasma dynamics there. A choked plasma flow is expected around the tube exit. Two other distinguished processes take place in the magnetic nozzle: the supersonic plasma acceleration and its magnetic interaction with the thruster, and the detachment from the magnetic nozzle. The four main processes are coupled but, in order to understand the main phenomena and parameters at play, some extra assumptions are commonly made in order to treat each process independently. Subsequent studies and numerical codes will look for a deeper and consistent coupling of the four independent models.

Beyond gaining insight in the plasma physics, a central goal of our research has been to understand well the thrust mechanism on an helicon thruster and to assess its propulsive capabilities. In order to compete with other plasma thrusters the helicon thruster must offer good figures for specific impulse, thrust efficiency, and thrust/weight ratio. The two first figures-of-merit are directly related to the plasma discharge. First, since the helicon thruster is basically an electrothermal accelerator, the specific impulse is proportional to the square root of the plasma internal energy. Therefore a high plasma temperature is needed; observe that this condition is not required for an helicon source for a non-propulsive application. Then, good thrust efficiency requires: (i) efficient wave-plasma energy conversion from the antenna, (ii) near-total plasma ionization inside the vessel, (iii) efficient plasma heating, with small energy losses to the walls, (iv) efficient conversion of internal energy into directed axial energy, minimizing plume divergence, and (v)

efficient plasma detachment. Each of these requirements can be measured with a dedicated efficiency parameter. Some of them will be discussed here.

Research in helicon thrusters has been much influenced by the Helicon Double Layer Thruster(HDLT) proposed by Charles and Boswell[6]. These authors first reported the formation of a current-free double layer (CFDL) near the interphase of an helicon source tube and a larger diffusion chamber[1] and related the presence of a supersonic ion beam to the jump in electric potential across the CFDL[7]. Based on this, they suggested that 'the CFDL in an expanding plasma could be the basis of an enhanced type of space plasma thruster'[1], referred later as the HDLT. The formation of a CFDL in the expanding plasma and its propulsive role will be commented here too.

3. Internal plasma dynamics

There is much theoretical research done on the interaction of the RF wave emitted by the antenna with the plasma[5, 8, 9, 10]. The most common analysis is to assume a normal wave with a time dependence $\propto (i\omega t)$ and to solve the Maxwell equations

$$\nabla \times \boldsymbol{E} = -i\omega \boldsymbol{B}, \quad \nabla \times \boldsymbol{B} = i\omega \bar{\bar{\epsilon}} \cdot \boldsymbol{E}, \tag{1}$$

where the dielectric tensor $\bar{\bar{\epsilon}}(\boldsymbol{r})$ carries all the plasma information through its density $n_e(\boldsymbol{r})$ and collision-frequency functions. The basic dispersion relation for a *uniform and infinite* plasma shows that two pairs of modes, helicon and Trievelpiece-Gould(TG) waves, can propagate. Analyses for bounded, nonuniform plasmas are limited generally to 1D, radial models. The plasma-wave response depends mainly on the wave frequency ω, the magnetic field strength B_0 and the plasma density. Resonant absorption of the RF emission is most efficient in the parametric region where the two pairs of modes propagate within the plasma column (i.e. they are not evanescent), interact with each other, and absorption takes place preferentially through the TG modes and near the plasma edge. This is called the *helicon or blue mode* in contrast to the *inductive mode*, when the waves penetrate evanescently within the plasma.

The 2D dynamics of the plasma inside the source depends on the vessel dimensions, the topology of the applied magnetic field, the flow of injected gas into the vessel $\dot{m}$, and the spatial distribution of power absorbed from the wave, $p_a(\boldsymbol{r})$. Functions $p_a(\boldsymbol{r})$ and $n_e(\boldsymbol{r})$ couple the plasma-dynamics and the plasma-wave interaction problems. The goals of the plasma dynamics study are to determine: the plasma density profile, the plasma conditions at the vessel exit –which constitute the upstream conditions for the supersonic plasma acceleration in the magnetic nozzle–, the propellant utilization η_u –which should be high for efficient thruster operation–, the internal efficiency or ratio between useful power and absorbed power, and the influence of the different governing parameters on the above magnitudes –in order to optimize the design and operation of the thruster–.

3.1 Radial structure

In order to define a model tractable analytically we have assumed that the magnetic field is axial and constant and the plasma temperature is constant. A variable-separation technique, already implemented successfully for the plasma discharge in a Hall thruster[11], has been used here to decouple partially the radial and axial dynamics, which still remain coupled through the local plasma recombination frequency at the lateral walls of the vessel.

The analysis of the radial model is detailed in Ref.[12]. The model invokes: the zero-Debye length limit –in order to separate the Debye sheath and quasineutral plasma regions– and the zero-beta limit (beta is the thermal-to-magnetic pressure ratio) –in order to neglect the magnetic field induced by azimuthal plasma currents–. Then, the quasineutral response is characterized by three-dimensionless parameters, relating the electron gyroradius ℓ_e, the electron collision mean-free-path λ_e, and the ion collision mean-free-path λ_i, to the tube radius R. Three parametric regimes are distinguished: the unmagnetized regime, the main magnetized regime, and, for a low-collisionality plasma, an intermediate-magnetization regime. The helicon source is expected to operate within the main magnetized regime with

$$\lambda_d \ll \ell_e \ll R \sim \lambda_e, \lambda_i,$$

with λ_d the Debye length. The plasma radial structure in that regime consists of a diffusive region occupying the bulk of the tube, followed by a quasineutral inertial layer and the Debye sheath. The typical thicknesses of these two layers are ℓ_e and λ_d.

The plasma response in the bulk diffusive region is characterized by (a) small plasma radial drift u_r and small ambipolar electric field, (b) negligible ion azimuthal drift, (c) a large azimuthal electron drift $u_{\theta e}$, and (d) the near

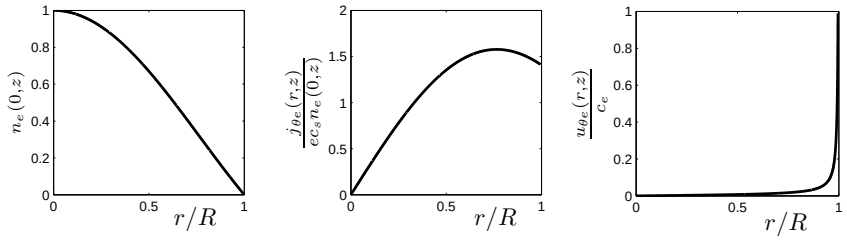

Figure 1: Typical radial profiles for the bulk diffusive region[12].

balance of the expanding electron pressure gradient and the confining magnetic force created by $u_{\theta e}$ –as in z-pinch equilibrium–. The radial profiles, plotted in Fig.1, satisfy

$$\frac{n_e(r,z)}{n_0} = J_0\left(a_0\frac{r}{R}\right), \qquad \frac{u_{\theta e}(r,z)}{c_e} = \frac{\ell_e}{R}a_0\frac{J_1\left(a_0 r/R\right)}{J_0\left(a_0 r/R\right)}, \qquad \frac{u_r(r,z)}{c_s} = \frac{u_{\theta e}}{c_e}\frac{\ell_e}{\lambda_e}, \tag{2}$$

with: $n_0 = n_0(0,z)$ the density profile at the plasma axis; $\lambda_e = \lambda_e(z)$ the collision mean-free path averaged radially; $c_s = \sqrt{T_e/m_i}$, $c_e = \sqrt{T_e/m_e}$; J_0 and J_1 Bessel functions and $a_0 \simeq 2.405$ the first zero of J_0. Notice that u_r is normalized with $c_s = \sqrt{T_e/m_i}$ and $u_{\theta e}$ with $c_e = \sqrt{T_e/m_e}$.

The transition to the inertial layer occurs when $u_{\theta e} \sim c_e$ and is characterized by electron-inertia effects limiting further increments of $u_{\theta e}$. Ion inertia is limited to a thinner sublayer, where the transition from magnetically-confined to electrostatically-confined electrons takes place. This assures also a gentle transition to the Debye sheath.

The large electron azimuthal energy in the inertial layer yields a relevant contribution to the plasma energy deposited in lateral walls. Nonetheless, these energy losses to the wall are moderate or small because of the strong magnetic confinement, which implies a large radial decay in plasma density: the plasma flux to the wall scales proportional to $\ell_e^2/(R\lambda_e)$. The large density gradient near the wall can have some relevant effect on the plasma-wave conversion via the Trivelpiece-Gould waves, but this aspect has not been investigated.

It will be found that competitive helicon thrusters require a high plasma temperature, a relatively-high density, and a moderate magnetic field. These are conditions that make the plasma beta, $\beta = n_e T_e \mu_0/B^2$, non negligible. The analysis of Ref.[12] has been extended in Ref.[13] to the non-zero beta case, when the magnetic field induced by the azimuthal plasma current tends to demagnetize partially the plasma. Then, the plasma response is characterized mainly by two dimensionless parameters, which are proportional to the electron gyroradius and the electron skin-depth, d_e, and each of them measures the independent influence of the applied magnetic field and the plasma density. The strong magnetic confinement regime, characterized by very small wall losses, is limited to the small gyroradius and large skin-depth ranges. In the high-density case, when the electron skin-depth is smaller than the gyroradius, the plasma behaves as unmagnetized and is confined only electrostatically. Therefore, the skin-depth turns out to be the magnetic screening length of this stationary plasma column.

3.2 Axial structure

The axial model is analyzed in Ref. [14], based on a previous model by Fruchtman[15]. It works with r-averaged magnitudes and determines, first, the plasma formation and neutral depletion, and second, the plasma flow towards both the tube rear-end and front exit. Sonic plasma conditions apply at both tube ends. At the back plate a Debye sheath forms and the plasma recombines. Ion collisions on the plasma flow are found negligible but they can affect neutral dynamics. Minimum conditions in terms of plasma flow, tube length, and plasma temperature in order to achieve near-total ionization are derived. The power losses to the lateral wall depend strongly on the magnetic confinement, and they can be reduced to be a marginal effect for reasonable values of the magnetic strength. Figure 2, from Ref.[14], shows (in dimensionless form) typical axial plasma profiles: the plasma velocity is sonic at the tube exit and backwards-sonic at the edge of the rear Debye sheath; plasma density presents a maximum around the location where the plasma flow changes direction; the neutral density decrement represents gas ionization; and ν_w is the plasma recombination frequency at the wall, measuring wall losses.

The plasma temperature is assumed constant in the vessel. This simplification has some experimental support and allows us to use a global energy balance, independent of the details of the 2D map of the absorbed power density,

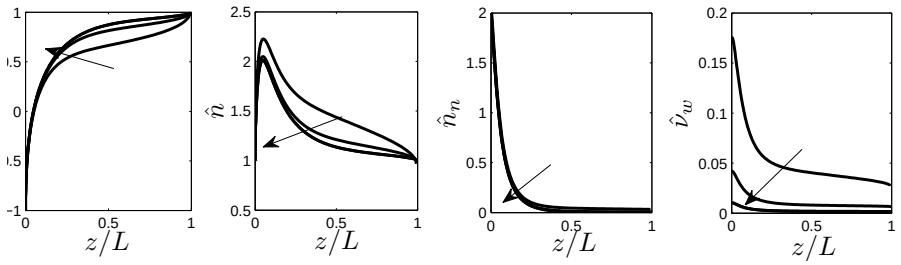

Figure 2: Typical axial profiles in dimensionless form for different values of the axial magnetic field (increasing along the arrows)[14].

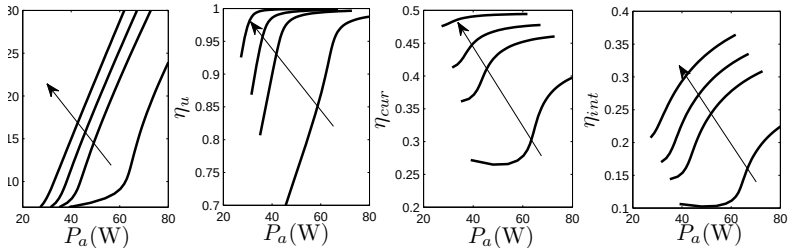

Figure 3: Performance of the plasma source versus the total power absorbed from the RF wave for different magnetic strengths (increasing along the arrows)[14].

to determine the plasma temperature. The energy balance yields

$$P_a = P_{ion} + P_W + P_A + P_E, \tag{3}$$

where the absorbed power $P_a = \int p_a(\boldsymbol{r})d\boldsymbol{r}$ is distributed into ionization power P_{ion}, power losses to the lateral wall P_W, power losses to the back plate P_A, and useful power at the tube exit P_E. Indeed, Eq. (3) determines the plasma temperature. If magnetic confinement is adequate wall losses are small and one has

$$P_a \simeq \eta_u \frac{\dot{m}}{m_i} 2\Big[3T_e + E'_{ion}(T_e)\Big], \tag{4}$$

with E'_{ion} the effective ionization energy of the gas (including excitation/radiation losses).

The contribution of the helicon source to thrust efficiency is

$$\eta_{int}(T_e) = \frac{P_E}{P_a} \approx \frac{\eta_{cur}}{1 + E'_{ion}/(3T_e)}, \qquad \eta_{cur} = \frac{I_E}{I} \tag{5}$$

with I the total current of plasma produced and I_E the current at the source exit. The expression for η_{int} indicates that, since the helicon thruster is basically an electrothermal thruster (where the directed axial energy of the downstream plasma jet comes from the internal plasma energy) the plasma temperature must be high in order that the thrust efficiency be acceptable.

Figure 3 plots plasma performances. The functional relation between T_e and P_a comes from Eq. (3). As the magnetic field is increased losses to the tube walls decrease and larger values of T_e are obtained for the same absorbed power. Observe that near total ionization is easily achieved but the current efficiency η_{cur} is quite low. This is due to the simple magnetic configuration assumed in the model, where there is not magnetic confinement at the tube rear-end. As a consequence, $I_A \simeq I_E$, $\eta_{cur} < 0.5$, and energy losses at the rear end are unacceptably large. Hence, some kind of magnetic confinement (e.g. a magnetic mirror) must be placed there.

4. Plasma expansion in a magnetic nozzle

4.1 Plasma acceleration and thrust transmission

In addition to the helicon thruster, axisymmetric magnetic nozzles, created by an external set of coils, are being used in different propulsion devices under research, such as the Applied-Field MagnetoPlasmaDynamic Thruster[16], the

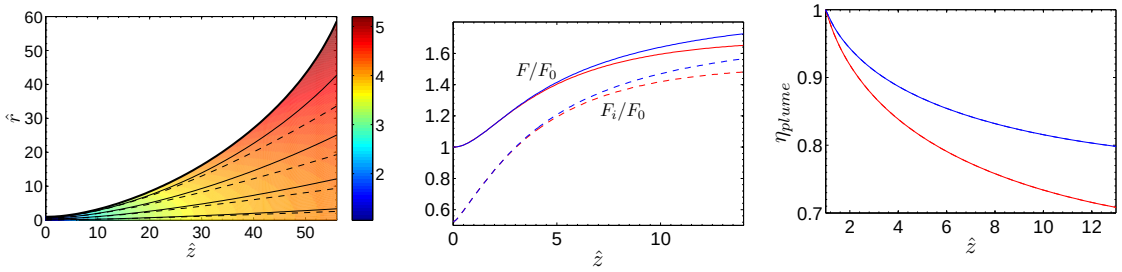

Figure 4: (Left)Magnetic/electron streamtubes (solid) and ion streamtubes (dashed); the color map represents the plasma Mach number, and the radial increase of M is due to plasma rarefaction. (Center) F/F_0 is the thrust gain along the divergent magnetic nozzle; F_i/F_0 is the ratio of ion-momentum-thrust to total-thrust at the nozzle throat; blue and red lines represent two different cases. (Right) Plume efficiency as ratio of axial-to-total energy flux of ions at different sections of the nozzle.

VASIMR[17], and the Divergent Cusp Field Thruster[18]. There is a simple analogy between the acceleration of a magnetized plasma in a magnetic nozzle and of a neutral gas in a solid (deLaval) nozzle. In both cases, the plasma flow has a regular sonic transition at the nozzle throat and accelerates supersonically afterwards. However, plasma physics in a magnetic nozzle are far more complex than gas dynamics in a solid nozzle, because of the different plasma energy forms, plasma azimuthal currents, self-magnetic fields, and the plasma detachment issue.

Ref.[19] presents a 2D model of the expansion of a collisionless plasma in a divergent magnetic nozzle, in the limit of magnetically-guided electrons and zero-beta. Thus, magnetic streamtubes are the streamtubes of electrons. However, ions, which are usually weakly magnetized and have a large inertia, present less divergent streamtubes except at the plasma-vacuum edge, which defines the magnetic nozzle shape [Fig. 4(left)]. This separation of ion and electron streamtubes creates small longitudinal currents, breaking current ambipolarity even if the plasma is globally current-free. It also imparts a slight azimuthal rotation to ions. Nonetheless, the main azimuthal or Hall current is the one due to electrons. This creates (perpendicular to the magnetic lines) a confining magnetic force that balances the pressure gradient at the nozzle throat. More downstream, an ambipolar electric field perpendicular to the magnetic lines is formed[20] which, on the one hand, bends the ion streamtubes towards the electron streamtubes and increments plasma radial rarefaction –this was already high because of the magnetic confinement–.

The two functions of a divergent solid nozzle on a neutral gas are (i) the conversion of thermal energy into directed kinetic energy, and (ii) a thrust gain through the pressure on the nozzle walls. Two equivalent processes take place in a magnetic nozzle. First, ions gain directed kinetic energy from conversion of the electron thermal pressure, via the ambipolar electric field. Second, there is a thrust gain but, since the magnetic nozzle has no walls, the mechanism is not a contact force (i.e. the plasma pressure) but the magnetic reaction force of the plasma current on the magnetic circuit of the thruster. These are illustrated in Fig. 4(center). Figure 4(right) shows the plume or nozzle efficiency as the ratio of axial-to-total power on ions. The plasma performance in the nozzle, both in terms of thrust gain and nozzle efficiency, is favored by a weak magnetization when radial rarefaction of the plasma beam is lower. Nozzles with low divergence-rates are also better in terms of plasma performances but require heavier and bulkier coils.

The main contribution of the azimuthal plasma current comes from electrons and is diamagnetic. The small ion contribution is paramagnetic and has a negative impact on thrust. Figure 5(a) shows the correct directions of the circuit and plasma currents in a propulsive magnetic nozzle and the action and reaction forces they exert; notice that this is a clear example of the basic law that currents running in opposite directions repel each other. The case of Fig. 5(b) would lead to plasma deceleration within the nozzle at the cost of reducing thrust.

4.2 Plasma detachment

The magnetic nozzle is an excellent vehicle to accelerate supersonically a plasma jet without wall contact. But once this is achieved, it is a burden since the beam needs to detach from the magnetic lines; otherwise, the beam would accelerate radially and turn back towards the thruster structure.

Reference[21] makes a detachment analysis based on the nozzle model of Ref.[19]. The detachment mechanisms proposed in the literature can be grouped in two types: *diffusive detachment* and *magnetic stretching*. Diffusive

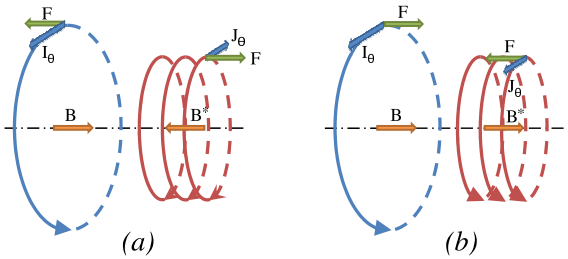

Figure 5: (a) Circuit and plasma currents for a propulsive magnetic nozzle. (b) Circuit and plasma currents leading to magnetic stretching, not found in a propulsive magnetic nozzle.

detachment can be caused by either plasma resistivity [22] or electron-inertia[23] and existing studies consider that the plasma beam detaches inwardly or convergently from the magnetic nozzle. However, we have shown, based on the azimuthal momentum equation for electrons, that electron diffusion by any of these two effects leads to outwards or divergent detachment, which is undesirable.

Detachment via magnetic strectching[24] was proposed for high-density plasma, with non-zero beta. It assumes that the induced magnetic field increments the applied field, thus stretching the effective magnetic nozzle. The plasma beam, by remaining attached to the resulting magnetic nozzle, would detach effectively and inwardly from the applied magnetic nozzle. Again, we have shown that this mechanism does not apply to a propulsive magnetic nozzle. The argument is quite simple: for the case of interest, sketched in Fig. 5(a), when plasma currents are diamagnetic, the induced magnetic field opposes the applied field, and therefore the resulting magnetic nozzle is more divergent than the one due to the applied field exclusively. Magnetic stretching would correspond to Fig. 5(b) which is not of application here.

Hence, our detachment analysis in a propulsive magnetic nozzle concludes that a major revision of the subject is necessary in order to identify the correct mechanism for convergent detachment. Our analysis suggests two basic processes as possible alternatives. The first one is simply *plasma demagnetization*, which here means electron demagnetization and would be caused by the opposite signs of the applied and induced magnetic fields and the increase of the induced-to-applied magnetic field ratio as the plasma moves downstream. The second alternative would be *electrostatic separation* and relies on the large radial rarefaction of the plasma which increases dramatically as the turning point of the magnetic nozzle is approached. This can cause the breaking of the quasineutrality condition so that the ion beam detaches from the electron beam. Further work on these detachment mechanisms is in progress.

5. Current-free double layers

Charles and Boswell found that sometimes a CFDL forms in the plume emitted by a helicon source and claimed it to constitute a novel and efficient acceleration mechanism. Previous studies and experiments on CFDLs had shown that they always form in plasmas with two electronegative species of disparate temperatures (cold and hot electrons or cold ions and hot electrons). Also, three different types of CFDLs exist depending on the entrance and exit conditions of the flow.

References [25] and [26] discussed a quasi-1D model of the acceleration of a three-species plasma (i.e. with two electron populations of different temperatures) in a convergent-divergent nozzle with the aim to understand and characterize the non-neutral CFDL and, its gentler form, the quasineutral steepened layer (QSL). It was shown that these structure appear as a consequence of the anomalous thermodynamics of a 3-species plasma. As the ambipolar electric potential decreases downstream the cold electron population is confined more strongly than the hot one. Therefore, although the cold population is expected to dominate the plasma density upstream, the hot population ends dominating downstream. Since the electric field is proportional to the local plasma temperature, a profile steepening occurs when the hot population becomes dominant, which we call a QSL.

For a simple plasma –without hot electrons– the sound speed is constant and the plasma undergoes a sonic transition at the magnetic nozzle throat. For a three-species plasma, the plasma Mach number is also 1 at the throat but the Mach number function can be nonmonotonic because of the sound speed changes with the local electron temperature. For small populations of very hot electrons, the supersonic Mach number function in the divergent side of the nozzle presents a minimum. The change of structure, from a QSL to a CFDL (which is a discontinuous surface in

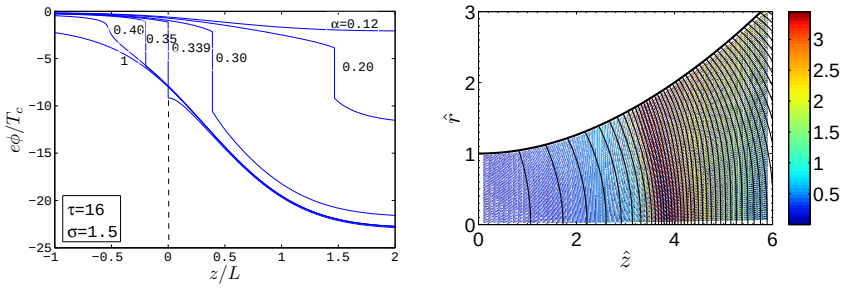

Figure 6: (Left) QSL and DL formation in an expanding plasma from the quasi-1D model; α is the upstream hot-to-cold electron ratios for density and temperature, respectively; σ characterizes the nozzle expansion area. (Right) Maps of the ambipolar electric field and equipotential lines, illustrating the presence of a QSL from the 2D nozzle for $\tau = 9$.

the quasineutral scale), happens when that minimum tends to be subsonic and the quasineutral plasma cannot manage, with a regular solution, three sonic points.

The parametric regions, in terms of density and temperature ratios between the two electron populations, for the QSL and the CFDL were determined. The QSL/CFDL location moves upstream as the density ratio increases, as Fig. 6(left) illustrates. Apart from the fulfilment or not of quasineutrality, a CFDL and a QSL do not differ much. Any difference is further blurred because the CFDL is a weak DL, that is one with a small percentage of relative charge separation, which extends tens or hundreds of Debye lengths.

Reference [27] generalizes the 2D model of the magnetic nozzle of Ref.[19] to include plasmas with two electron populations. This has allowed us to observe the 2D structure of a QSL [Fig. 6(right)]. Apart from recovering the 1D axial properties, the curved shape of the QSL and the nozzle efficiency were determined. The 2D model, being fully quasineutral, was not able to treat the CFDL.

The CFDL is certainly an interesting entity in plasma physics studies. However, for helicon thrusters, its interest lies in how it changes the plasma response and specifically on whether there is a gain in the propulsive capabilities of the device. Charles and Boswell base their prospects in the HDLT on the fact that ions are greatly accelerated across a CFDL. However it is known that the total plasma momentum remains unchanged across a DL[28, 29]: within the DL there is just a transfer of electron momentum to ion momentum. Therefore there is no thrust gain associated to the formation of a CFDL. All thrust gain in the divergent magnetic nozzle comes from the magnetic force of the plasma azimuthal currents, and the CFDL do not seem to change them. Any variation in propulsive efficiency in a three species plasmas (compared with a simple plasma with the same absorbed power) is marginal and due to details of the electron distribution function. Indeed, our studies with 1D and 2D models detect, in general, a small efficiency loss in a 3-species plasma.

6. Conclusions

The theoretical investigation reported here has provided much insight into the multiple processes shaping the plasma dynamics in the production and acceleration stages of an helicon thruster. To a large extent, the dominant phenomena, parameters, and regimes have been identified. The most complete and interesting analyses are on the plasma expansion and detachment in a magnetic nozzle and the formation of current-free double layers. Further and more detailed investigation will be better accomplished with more general models, which require more intensive numerical tools, transiting from what is considered a theoretical model to a simulation code.

Acknowledgments

This work was supported by the Gobierno de España (Project AYA-2010-16699). The author thanks Mario Merino for providing some of the figures.

References

[1] C. Charles and R. Boswell, Applied Physics Letters **82**, 1356 (2003).

[2] T. Ziemba, J. Carscadden, J. Slough, J. Prager, and R. Winglee, High Power Helicon Thruster, in *41th Joint Propulsion Conference, Tucson, AR*, AIAA paper 2005-4119.

[3] O. Batishchev, IEEE Transaction on Plasma Science **37**, 1563 (2009).

[4] D. Pavarin and others, Design of 50W Helicon Plasma Thruster, in *31th International Electric Propulsion Conference, Ann Arbor, Michigan, USA*, IEPC paper 2009-205.

[5] R. Boswell, Plasma physics and controlled fusion **26**, 1147 (1984).

[6] C. Charles, R. Boswell, and M. Lieberman, Applied Physics Letters **89**, 261503 (2006).

[7] C. Charles and R. Boswell, Physics of Plasmas **11**, 1706 (2004).

[8] K. Shamrai and V. Taranov, Plasma Physics and Controlled Fusion **36**, 1719 (1994).

[9] F. Chen, Physics of Plasmas **3**, 1783 (1996).

[10] D. Arnush and F. Chen, Physics of Plasmas **5**, 1239 (1998).

[11] E. Ahedo, J. Gallardo, and M. Martínez-Sánchez, Physics of Plasmas **10**, 3397 (2003).

[12] E. Ahedo, Physics of Plasmas **16**, 113503 (2009).

[13] E. Ahedo, Physics of Plasmas(submitted) (2011).

[14] E. Ahedo, Cylindrical model of a helicon-generated plasma, in *31th International Electric Propulsion Conference, Ann Arbor, Michigan, USA*, IEPC paper 2009-193.

[15] A. Fruchtman, G. Makrinich, and J. Ashkenazy, Plasma Sources Science and Technology **14**, 152 (2005).

[16] G. Krülle, M. Auweter-Kurtz, and A. Sasoh, J. Propulsion and Power **14**, 754 (1998).

[17] F. R. C. Diaz, J. P. Squire, R. D. Bengtson, B. N. Breizman, F. W. Baity, and M. D. Carter, The Physics and Engineering of the VASIMR Engine, in *36th Joint Propulsion Conference, Huntsville, Alabama*, AIAA paper 2000-3756.

[18] D. Courtney and M. Martínez-Sánchez, Diverging Cusped-Field Hall Thruster, in *30th International Electric Propulsion Conference, Florence, Italy*, IEPC paper 2007-039.

[19] E. Ahedo and M. Merino, Physics of Plasmas **17**, 073501 (2010).

[20] M. Merino and E. Ahedo, IEEE Transactions Plasma Science (accepted) (2011).

[21] E. Ahedo and M. Merino, Physics of Plasmas (accepted) (2011).

[22] R. W. Moses, R. Gerwin, and K. Schoenberg, Resistive plasma detachment in nozzle based coaxial thrusters, in *Proceedings Ninth Symposium on Space Nuclear Power Systems, Albuquerque, New Mexico, 1992*, AIP Conference Proceedings No. 246, pp. 1293–1303, American Institute of Physics, Woodbury NY, 1992.

[23] E. B. Hooper, Journal of Propulsion and Power **9**, 757 (1993).

[24] A. Arefiev and B. Breizman, Physics of Plasmas **12**, 043504 (2005).

[25] E. Ahedo and M. Martínez-Sánchez, Physical Review Letters **103**, 135002 (2009).

[26] E. Ahedo, Physics of Plasmas **18**, 033510 (2011).

[27] M. Merino, 2d plasma flow in a magnetic nozzle with a bi-modal electron energy distribution function, Presented at the 7th AIAA-Pegasus Student Conference, Torino, Italy, 2011.

[28] M. A. Raadu, Physics Reports **178**, 25 (1989).

[29] A. Fruchtman, Physical Review Letters **96**, 065002 (2006).